JMATPRO	Journal of Advanced Materials and Processing 10 (3): 3-19, Summer 2022 http://jmatpro.iaun.iau.ir 20.1001.1.2322388.2022.10.3.1.8

Research Paper

Chemical Reaction, Substructure, and Mechanical Behavior of Spinel $MgAl_2O_4$, Mullite, and Forsterite Nanocrystallines by Applying Mechanochemical Process and Subsequent Three-Step Heat Treatment

Habib Fazelinezhad[1], Kourosh Hormozi[1], Iman Emami[1], Saeid Jabbarzare[2*], Ahmad Monshi[3]

1. Department of Materials Engineering, Ahvaz Branch, Islamic Azad University, Ahvaz, Iran
2. Advanced Materials Research Center, Department of Materials Engineering, Najafabad Branch, Islamic Azad University, Najafabad, Iran
3. Department of Materials Engineering, Isfahan University of Technology, Isfahan, Iran.

ARTICLE INFO

Article history:

Received 7 April 2022
Accepted 30 June 2022
Available online 1 July 2022

Keywords:
Forsterite
Mechanical behavior
Mullite
Spinel
Three-step heat treatment

ABSTRACT

This research aimed to evaluate the formation reaction, substructure, crystallite size, and mechanical behavior of spinel $MgAl_2O_4$, mullite, and forsterite nanocrystalline using a combination of mechano-chemical and three-step heat treatment. The main aim was achieved by decreasing the annealing temperature to the level of nanostructures and high mechanical strength by considering three-step heat treatment. We conducted the mechanism of these phases by considering low milling and declining annealing temperatures. More specifically, phase transformation was conducted with proper activation energy to form the nanocrystalline at 1050 ^oC. The obtained crystallite sizes for spinel $MgAl_2O_4$, mullite, and forsterite nanocrystallites were 49.5, 70.71, and 47.8 nm, respectively, and their substructure verified the formation of 50 nm nanocrystalline. It was revealed that mechanical strengths were in order of increasing 378.33, 216.33, and 179.66 MPa. Interestingly, spinel $MgAl_2O_4$ was outstanding compared to mullite and forsterite due to the strong comparison between ionic and covalent bonds and the breaking of silicate networks by alumina and magnesia in mullite and forsterite structures. Declining the annealing temperature by three-step heat treatment proved to help develop spinel, mullite, and forsterite, and enhance their mechanical strengths as potential substrates for porous materials, ceramics, and refractory industries.

Citation: Fazelinezhad, H.; Hormozi, K.; Emami, I.; Jabbarzare, S.; Monshi, A. (2022). Chemical Reaction, Substructure, and Mechanical Behavior of Spinel MgAl2O4, Mullite, and Forsterite Nanocrystallines by Applying Mechanochemical Process and Subsequent Three-Step Heat Treatment, Journal of Advanced Materials and Processing, 10 (3), 3-19. Dor: 20.1001.1.2322388.2022.10.3.1.8

[*] **Corresponding Author:**
E-Mail: saeid.jabbarzare@gmail.com

1. Introduction

Spinel $MgAl_2O_4$ has been utilized due to its unique properties of high specific strength in low and high temperatures, great chemical resistance, appropriate thermal shock, low thermal conductivity, great thermal expansion, and compatible chemical properties. Because of these great features, spinel $MgAl_2O_4$ is considered by engineers and designers as an ideal compound for the fabrication of traditional and technical ceramics such as shaped and shapeless refractory products for metallurgy, refractory, cement industries, electro-ceramics, and porous materials that are normally used in high-temperature applications [1-4]. Moreover, spinel $MgAl_2O_4$ is used as a refractory compound in steel and cement rotary furnaces and has a melting point of 2135 °C [1-4]. In addition, it is utilized due to its great optical and dielectric properties as well as high mechanical strength for applications such as catalysts and sensors [5, 6].

Likewise, mullite ($3Al_2O_3.2SiO_2$) is known to be an advanced ceramic for high-temperature applications in refractory and ceramics industries. It has special properties such as proper thermal shock, chemical stability, optimal bending strength, and high melting point as well as great chemical and physical properties [7-11]. Mullite also has widespread applications in refractories, catalysts, gas filters, and the fabrication of sensors and thermal insulations [12-14]. Moreover, since the dielectric constant of mullite is 6.7, it is appropriate for fabricating dielectric products [15, 16].

Forsterite is a form of crystalline magnesium silicate that is known as olivine groups. Its chemical formulation is Mg_2SiO_4 with a high melting point of about 1890 °C and is used in fabricating refractory and ceramic parts. Due to properties such as ideal physical and mechanical properties, great thermal conduction ability, proper chemical stability, and excellent insulation properties, it is considered as an outstanding refractory compound for application in ceramic and refractory industries [17-20].

Spinel $MgAl_2O_4$, mullite, and forsterite have recently attracted the attention of many researchers due to their numerous applications in various industries. The ceramics can now be synthesized by materials such as magnesia (MgO), alumina (Al_2O_3), magnesium carbonate ($MgCO_3$), aluminum and magnesium hydroxides $Mg(OH)_2$ and $Al(OH)_3$, silica (SiO_2), and salt [21-23]. Furthermore, they are being synthesized using different methods, including sol-gel, mechanochemical, electrospinning, and heat treatment techniques [24, 25]. The goal of the present research was to investigate the formation, crystallite size, substructure and mechanical behavior of spinel $MgAl_2O_4$, mullite, and forsterite nanocrystalline by applying mechano-chemical and subsequent three-step heat treatment. In other words, the major aim was accessing via declining the annealing temperature to the level of nanostructures and high mechanical strength by considering three-step heat treatment.

2. Materials and methods

2.1. Raw materials and synthesis of mullite, forsterite, and spinel $MgAl_2O_4$

Raw materials used included alumina (Al_2O_3) (Merck, 99% purity), magnesia (MgO) (Refractory Tuka, Iran and 90% purity), silica (SiO_2) (Merck, 98% purity), and talc ($Mg_3Si_4O_{10}(OH_2)$) (China, 75% purity). In order to synthesize nanoceramics, mechanochemical and subsequent three-step heat treatment techniques were used. The mechanochemical process was employed to synthesize spinel $MgAl_2O_4$ and mullite nanocrystalline with 0, 8, 16, and 24 h of milling points, the milling speed of 600 rpm, and the ball-to-powder weight ratio of 5:1 [25] using the following equations:

(1) $MgO + Al_2O_3 = MgAl_2O_4$

(2) $3Al_2O_3 + 2SiO_2 = 3Al_2O_3.\ 2SiO_2$

In addition, mechanochemical process was used to synthesize forsterite nanocrystalline with 0, 8, 16, 24, and 34 h of milling points, the milling speed of 600 rpm, ball-to-powder weight ratio of 5:1 using the following equation:

(3) $Mg_3Si_4O_{10}(OH)_2 + SiO_2 \rightarrow 3MgO.\ 4SiO_2.\ H_2O + SiO_2$

It should be noted that the type, diameter, and weight of the balls were zirconia, 20mm, and 30g, respectively. After mechano-chemical processes, the milled specimens were pressed under the pressure of 5 to 6 MPa to get bulk specimens. Subsequently, three-step heat treatment was carried out on the bulk specimens regarding the following steps:

(1) Increased the furnace temperature up to 1450 ℃ with the rate of 5 ℃/min for 40 min.

(2) Declined the furnace temperature up to 1250 ℃ with the rate of 5 ℃/min for 80 min.

(3) Declined the furnace temperature up to 1050 ℃ with the rate of 5 ℃/min for 160 min.

Afterward, the synthesized specimens were characterized and their mechanical behavior was evaluated. It is worth noting that all the specimens were annealed under similar temperature conditions and the main aim was to examine chemical reactions and mechanical behavior using three-step heat treatment at equal temperatures.

2.2. Characterization processes

The X-ray diffraction patterns were prepared using a Philips diffractometer model PW10 with Cu-Kα tube (λ=1.54018 and $10^o<2\theta<80^o$) to evaluate the developed phases of the synthesized specimens. In order to calculate the crystallite size of nano-ceramics, a modified Scherrer method was used [26].

The SEM images, EDX analyses, and X-ray maps of the synthesized specimens were prepared by scanning electron microscope (FEI, QUANTA, USA) in order to evaluate the nano-ceramics morphology and their related distribution of elements. The TEM images of the synthesized specimens were prepared in order to examine and estimate the substructure and crystallite sizes of the specimens. Mechanical behaviors of nano-ceramics were assessed using measurement of the compressive strength by a compressive strength device (Hounsfield H25KS, England) as per ASTM–D5024–95a standard.

2.3. Statistical analysis

All the experimental procedures were repeated three times, and the proper statistical analysis was conducted using IBM SPSS statistics (version.21.00 software). The $p<0.05$ value was also considered in order to evaluate the significant differences.

3. Results and discussion

Figs. 1(a-d) demonstrate the XRD patterns of the specimens milled at 0, 8, 16, and 24 h in order to organize the synthesis of spinel $MgAl_2O_4$. As can be noticed in Fig. 1(a), the corundum (Al_2O_3) (JCPDS 01-071-1125) and periclase (MgO) (JCPDS 01-087-0653) phases were observed before milling and at the zero hour. In Fig. 1(b), after 8 h of milling, corundum, and periclase phases could also be observed. However, in this step, after 8 h of milling, the diffusion of magnesia into alumina did not occur; that is, phase transformation to diffuse magnesia into alumina did not happen for the formation of the spinel $MgAl_2O_4$ phase.

In Fig. 1(c), the XRD pattern shows the corundum and periclase phases after 16 h of milling. Interestingly, the observed results were quite similar to those of the previous XRD patterns. It can therefore be stated that the milling process of up to 16 h between alumina and magnesia was insufficient to form the spinel $MgAl_2O_4$ phase since there was no diffusion between the compounds. As can be seen in Fig. 1(d), after 24 h of milling, only the corundum and periclase phases were noticed, which is quite similar to the obtained results in previous XRD patterns (Figs. 1(a-c)).

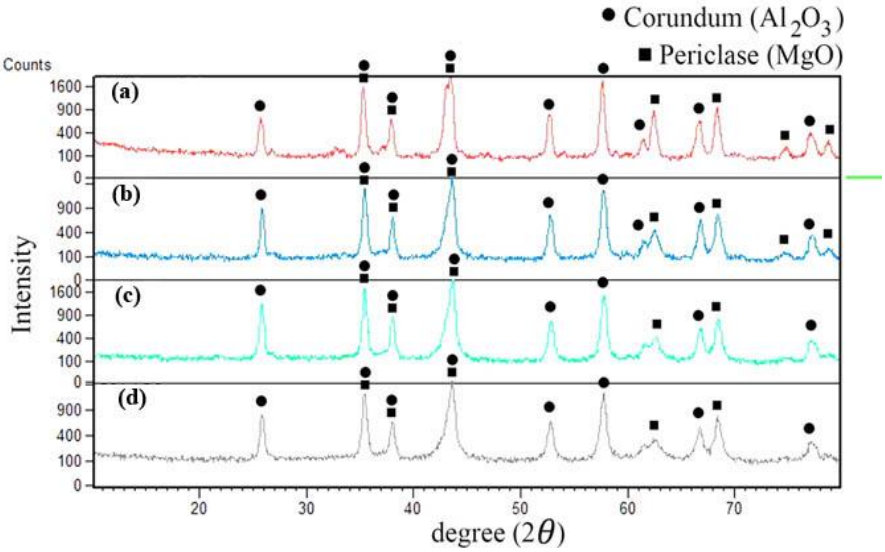

Fig. 1. XRD patterns of specimens milled: (a) 0 h, (b) 8 h, (c) 16 h and (d) 24 h to synthesize spinel $MgAl_2O_4$

In order to develop the spinel $MgAl_2O_4$ phase, a phase transformation was needed between magnesia and alumina. Magnesia diffuses into alumina in order for the transformation to occur. However, to form ceramics phases like spinel $MgAl_2O_4$, high activation energy was needed. Also, no phase transformation takes place merely from destruction of magnesia structure and its diffusion into alumina. This was to develop the spinel $MgAl_2O_4$ since special temperature conditions are not needed to be provided. Normally, in the milling process, strain energy will be reserved inside the particles, and preparation of the phase transformation will be grown in it so that the spinel $MgAl_2O_4$ phase is being formed.

Overall, it can be concluded that mechano-chemical process cannot be an effective method for the development of the spinel $MgAl_2O_4$ alone; rather, subsequent annealing is required for this purpose. The data in Figs. 2(a-c) illustrate the XRD patterns of the milled specimens annealed through three-step heat treatment. In the three XRD patterns, the spinel $MgAl_2O_4$ phase was verified in all peaks perfectly.

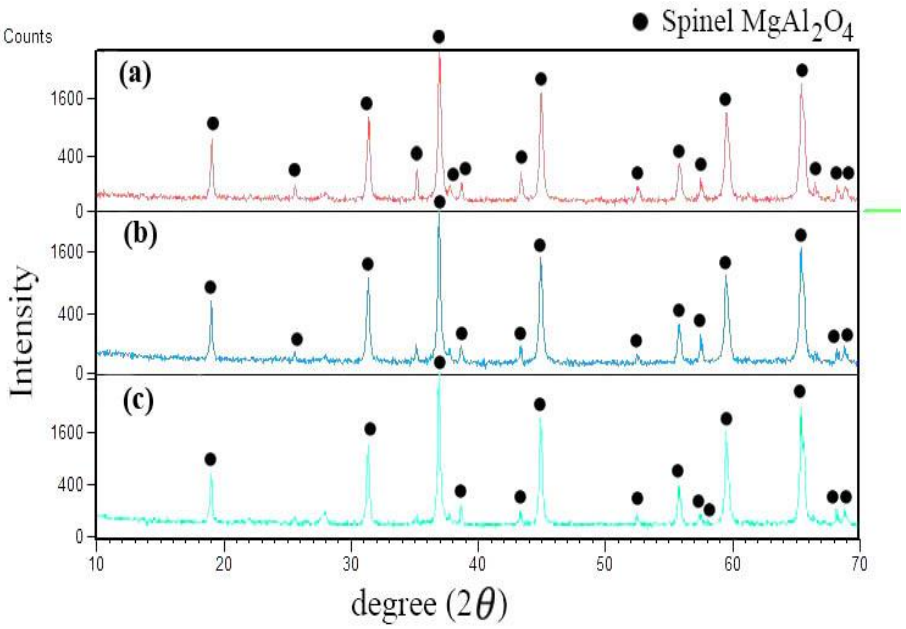

Fig. 2. XRD patterns of milled specimens annealed to synthesize spinel $MgAl_2O_4$: (a) 8 h, (b) 16 h and (c) 24 h

In other words, all peaks matched with the spinel $MgAl_2O_4$ phase (JCPDS 00-005-0672) to a large extent. It can be explained that the required activation energy was provided in an attempt to develop the spinel $MgAl_2O_4$ phase by conducting the three-step heat treatment and enhancing temperature up to 1450 ℃. Then, we noticed that the peaks related to the corundum and periclase phases disappeared and those related to the spinel $MgAl_2O_4$ phase appeared. Essential thermal energy was supplied in order to develop the activation energy and spinel $MgAl_2O_4$ nucleation at 1450 ℃. After the temperature was lowered to 1250℃, strain energy and growth of the nucleations happened so that the growth process could be continued after decreasing the temperature at 1050℃ and the spinel $MgAl_2O_4$ phase was developed completely. In other words, a stoichiometric ratio was used to form the spinel phase, and the phase transformation was made properly. The mechano-chemical and three-step heat treatment techniques rendered the development of the strain energy in the milling process. In the ball mill, the development of appropriate nuclear temperature is considered as the first step, the growth of spinel $MgAl_2O_4$ crystals as the second step (1250 ℃), and the formation of the spinel $MgAl_2O_4$ as the third step (1050 ℃). The steps are possibly comparable to the phase transformation during the spinel $MgAl_2O_4$ formation, which happened at higher than 1500 ℃ for several hours. Fig. 3 illustrates a schematic of the formation of spinel $MgAl_2O_4$.

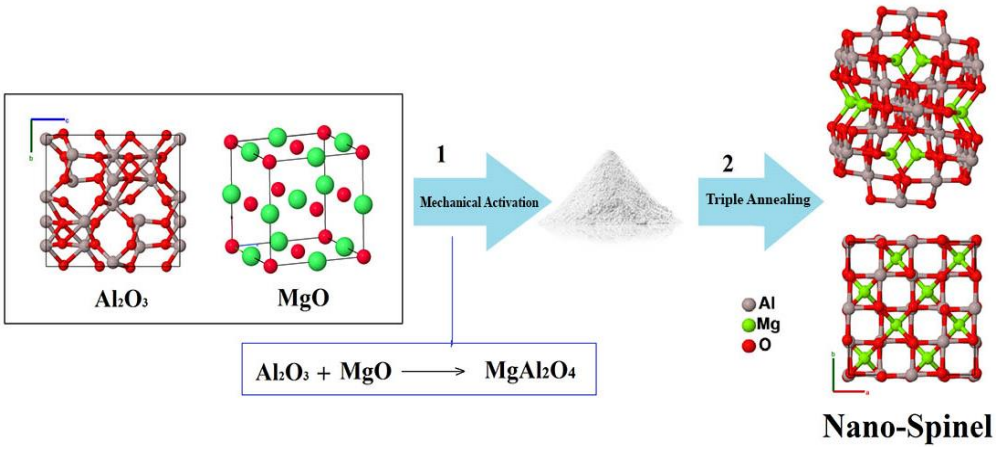

Fig. 3. A scheme of formation of spinel $MgAl_2O_4$

Figs. 4(a-d) illustrate the XRD patterns of the specimens milled at 0, 8, 16, and 24 h, respectively, to target the synthesis of mullite. The XRD patterns revealed corundum (Al_2O_3) (JCPDS 01-071-1127) and quartz (SiO_2) (JCPDS 00-001-0649), but mullite phase ($3Al_2O_3.2SiO_2$) was not noticed in the milled specimens as shown in Figs. 4(a-d). It is likely that the formation of mullite phase was subjected to a

phase transformation between silica (SiO_2) and alumina (Al_2O_3), and the transformation could be accomplished through the diffusion of silica into alumina. It is worth noting that high activation energy is required for the formation of ceramic compounds like the mullite, and phase transformation does not form the mullite only from destruction of silica structure and its diffusion into alumina structure if proper temperature conditions are provided. In the mechano-chemical process, strain energy is normally stored in the particles and phase transformation is performed in the heat treatment process just like the annealing technique. Figs. 5(a-c) show the XRD patterns that are related to the milled specimens annealed using three-step heat treatment. The XRD patterns clearly verified the formation of the mullite ($3Al_2O_3.2SiO_2$) phase (JCPDS 00-002-0431), which agrees with the peaks. The enhancement of temperature to 1450 ℃ in the three-step heat treatment process also helped the provision of activation energy to form the mullite phase so that after the three-step heat treatment, the corundum phase disappeared and the mullite phase appeared. Essential thermal energy was supplied at 1450 ℃ to develop the activation energy and mullite nucleation. The growth of nucleation was carried out at 1250 ℃, and the mullite phase was developed at 1050 ℃. In other words, phase transformation was perfectly conducted at about a stoichiometric ratio for the formation of the mullite phase. Fig. 6 shows a schematic of the mullite formation.

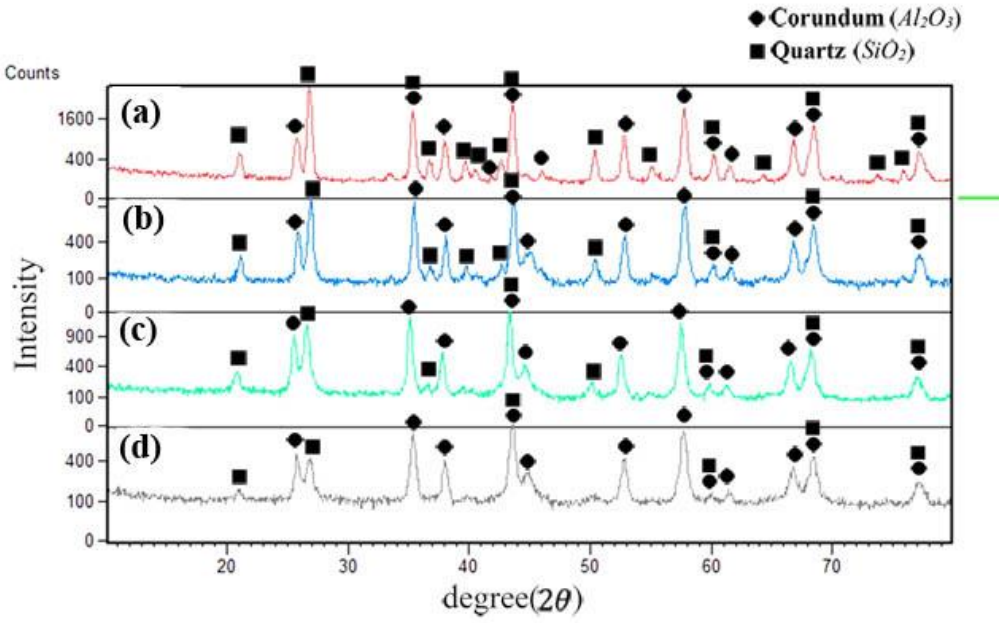

Fig. 4. XRD patterns of specimens milled: (a) 0 h, (b) 8 h, (c) 16 h and (d) 24 h to synthesize mullite

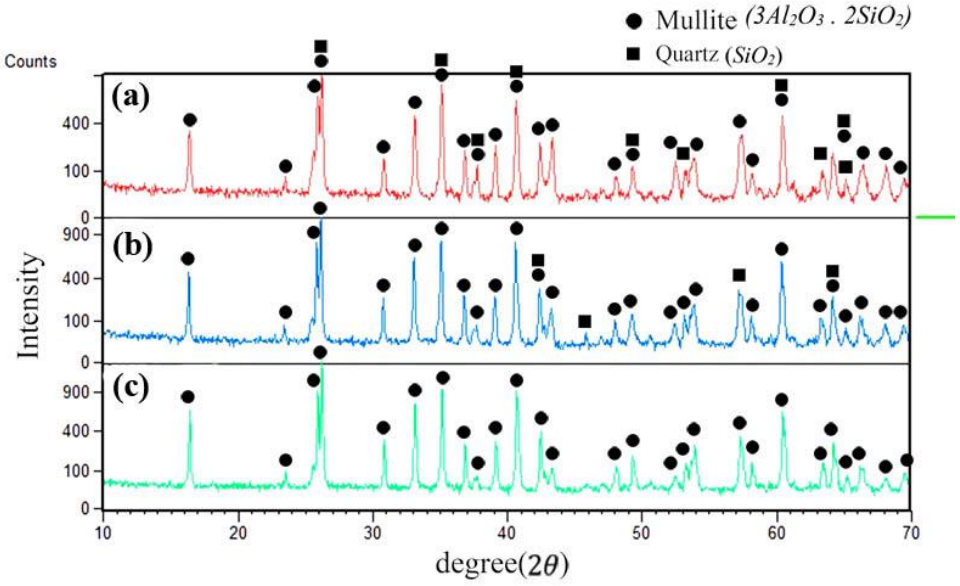

Fig. 5. XRD patterns of milled specimens annealed to synthesize mullite: (a) 8 h, (b) 16 h and (c) 24 h

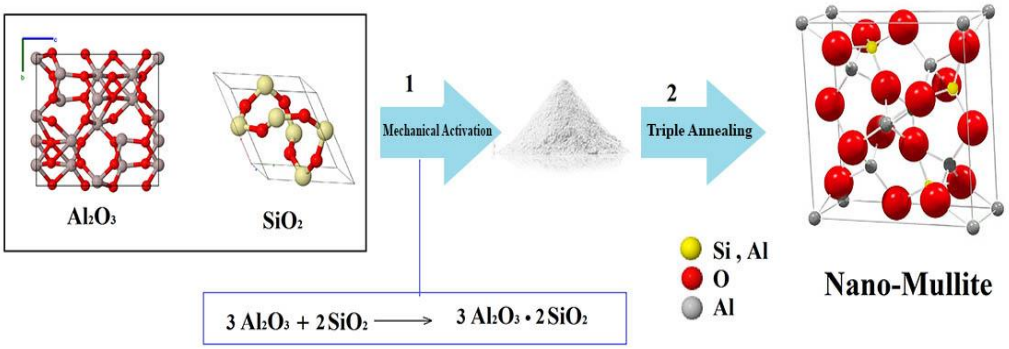

Fig. 6. A scheme of formation of mullite

The data in Figs. 7(a-d) illustrates the XRD patterns of the milled specimens at 0, 8, 16, and 24 h for the synthesis of forsterite. The results showed that the forsterite phase (Mg_2SiO_4) was not developed, but Talc ($Mg_3Si_4O_{10}(OH_2)$) (JCPDS 00-029-1493) and quartz (SiO_2) (JCPDS 01-085-0797) phases were noticed in the XRD patterns after the mechano-chemical process. Phase transformation is needed to develop the forsterite phase; in other words, silica must be diffused into talc structure and the process requires proper energy activation. This results in the conduction of heat treatment in order to achieve proper energy activation and to form forsterite. Figs. 8(a-c) shows the XRD patterns of the milled specimens annealed by using the three-step heat treatment method. Enstatite phase ($MgSiO_3$) (JCPDS 00-019-0768) was noticed in the XRD patterns. Talc and silica reacted enstatite and activation energy led to the reaction. Mechanical activation was repeated up to 34 h (milling) to reach the forsterite phase; then, three-step heat treatment was repeated. Fig. 9 shows the XRD pattern of milled specimen at 34 h that was annealed. Data in Fig. 9 verified the formation of the forsterite (Mg_2SiO_4) phase (JCPDS 01-071-0795). The proper activation energy was supplied in order to develop forsterite nucleation at 1450℃, and with the impact of the annealing process at 1250℃, the growth of forsterite crystals was carried out. Finally, forsterite was completely developed at 1050 ℃, which can be explained by the following equation:

(4) $MgSiO_3 + MgO = 2MgO.SiO_2$

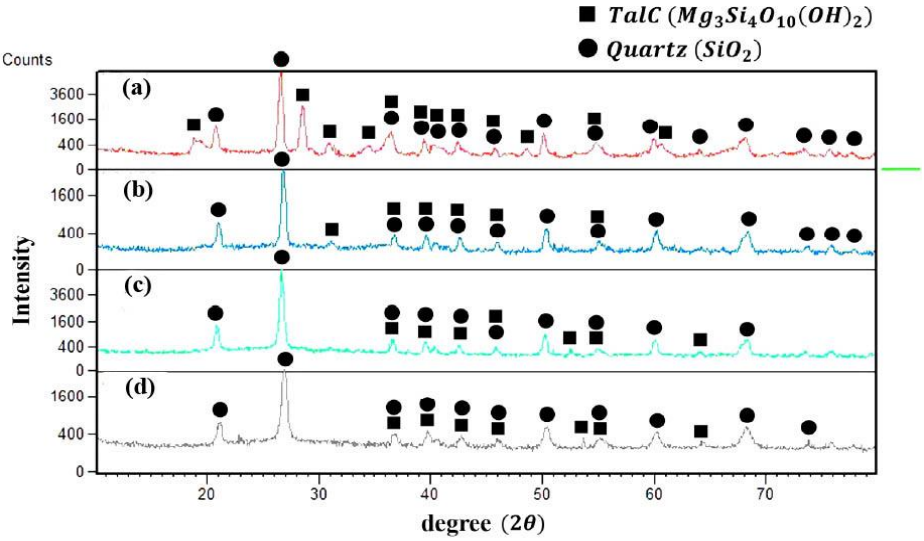

Fig. 7. XRD patterns of specimens milled: (a) 0 h, (b) 8 h, (c) 16 h and (d) 24 h to synthesize forsterite

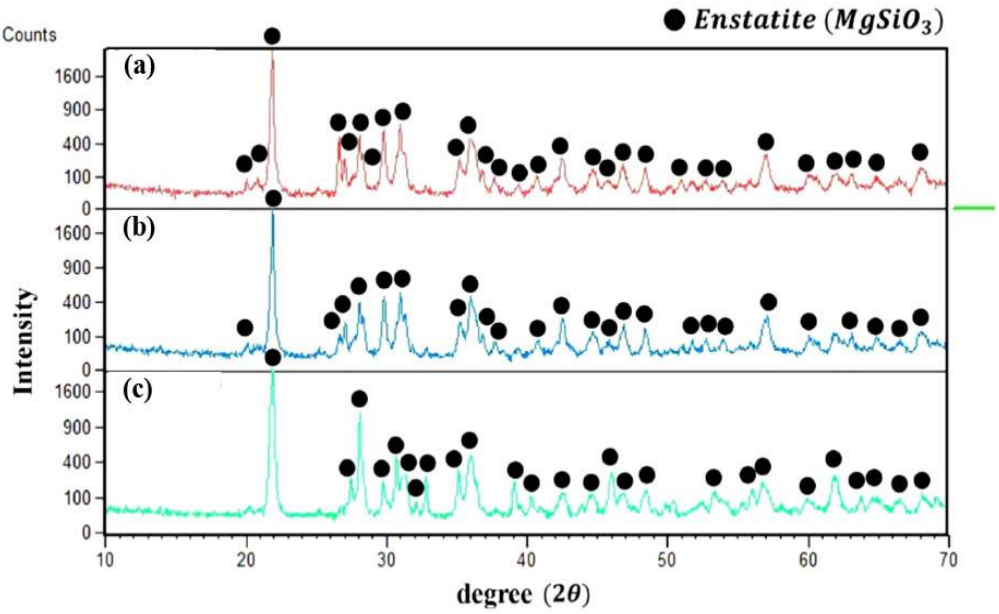

Fig. 8. XRD patterns of milled specimens annealed to synthesize forsterite: (a) 8 h, (b) 16 h and (c) 24 h

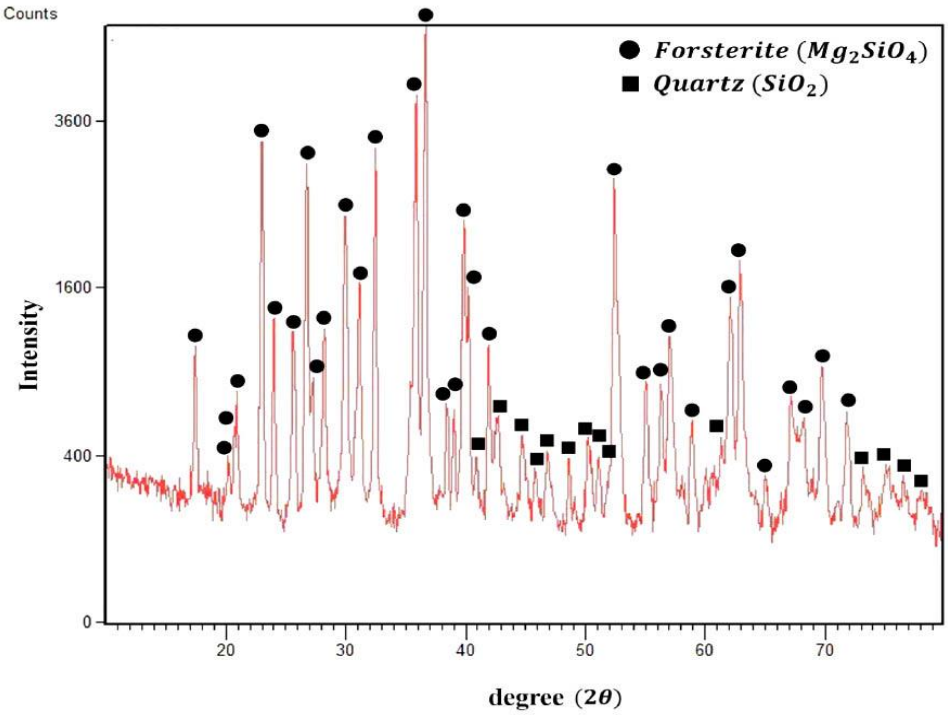

Fig. 9. XRD pattern of milled specimen (34 h) annealed to synthesize forsterite

Fig. 10 illustrates the schematic of the forsterite formation. The obtained results from phase analyses proved that synthesis of the spinel $MgAl_2O_4$, mullite, and forsterite was successful by applying a combination of mechano-chemical and subsequent three-step heat treatment techniques. Therefore, using low milled time in the milling process and, on declining annealing temperature using a three-step heat treatment technique could be considered as optimum techniques for the development of nano-ceramics in contrast to using high-temperature annealing for several hours.

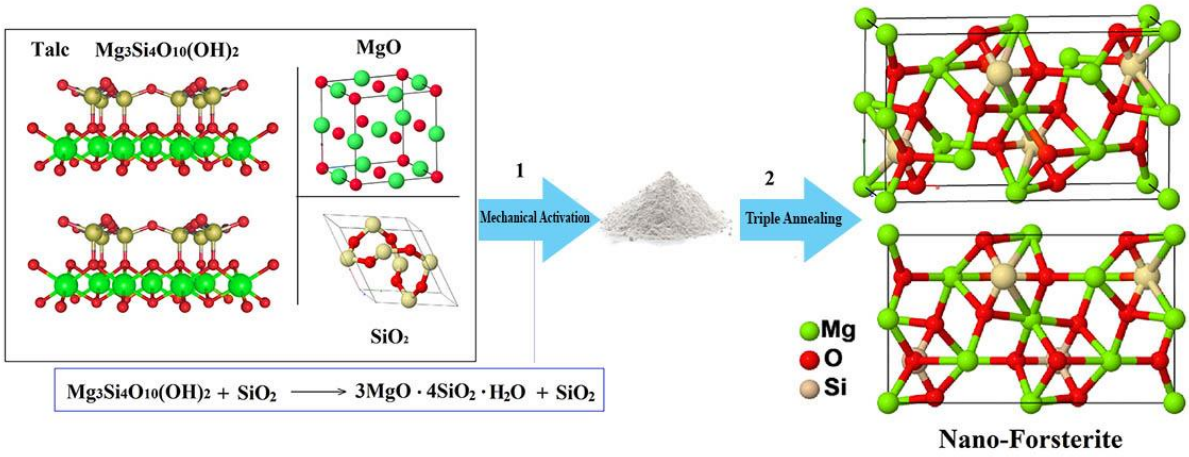

Fig. 10. A scheme of formation of forsterite

The crystallite size of the spinel $MgAl_2O_4$, mullite, and forsterite compounds was calculated via Modified Scherrer [26]. The crystallite sizes were obtained 49.5, 70.71, 47.8 nm for the spinel $MgAl_2O_4$, mullite, and forsterite, respectively. Fig. 11(a) presents SEM image of the spinel $MgAl_2O_4$ that rendered cluster crystals comprised of cubic–shaped particles. Fig. 11(b) and Table 1 exhibit the results of EDX analysis related to the spinel $MgAl_2O_4$. Results showed the non–availability of impurities in the synthesized spinel.

The weight percentages presented for O, Mg, and Al were 37.23, 19.92, and 48.86, respectively. After converting weight percentage to atomic percentage, atomic percentages of 49.4, 12.15, and 38.44 were obtained for O, Mg, and Al, respectively. It can be claimed that the presented atomic percentages are in full agreement with the atoms of the spinel $MgAl_2O_4$. Figs. 11(c-e) show the results of X-ray map of the synthesized spinel $MgAl_2O_4$ that illustrates the distribution of oxygen. The image showed that oxygen was supplied from alumina and magnesia, and it was invested in the spinel structure. Fig. 11(d) shows the distribution of magnesium (Mg^{2+}) in all areas, and it also proves that appropriate primary distribution of magnesia occurred before uniform spinel was developed. Similarly, the data in Fig. 11(e) shows the distribution of aluminum, and that Al^{3+} was distributed fairly well.

Table 1. Results of EDX analysis of spinel $MgAl_2O_4$

Element	Weight %	Atomic %	Net Int.
O K	37.23	49.4	524.55
Mg K	19.92	12.15	554.68
Al K	48.86	38.44	1921.97

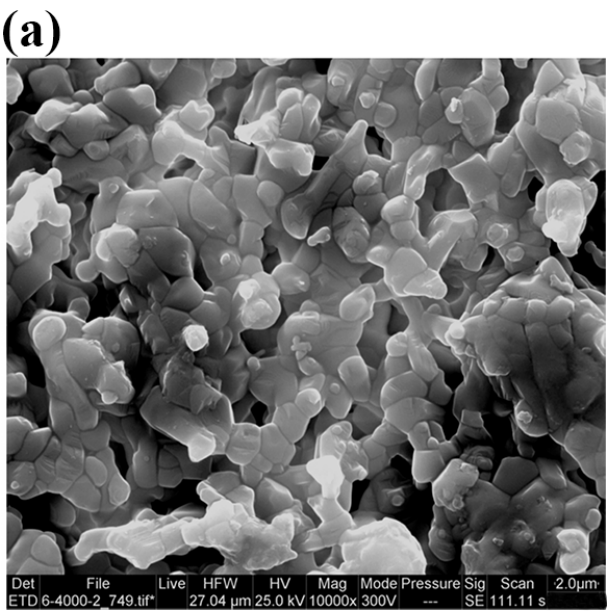

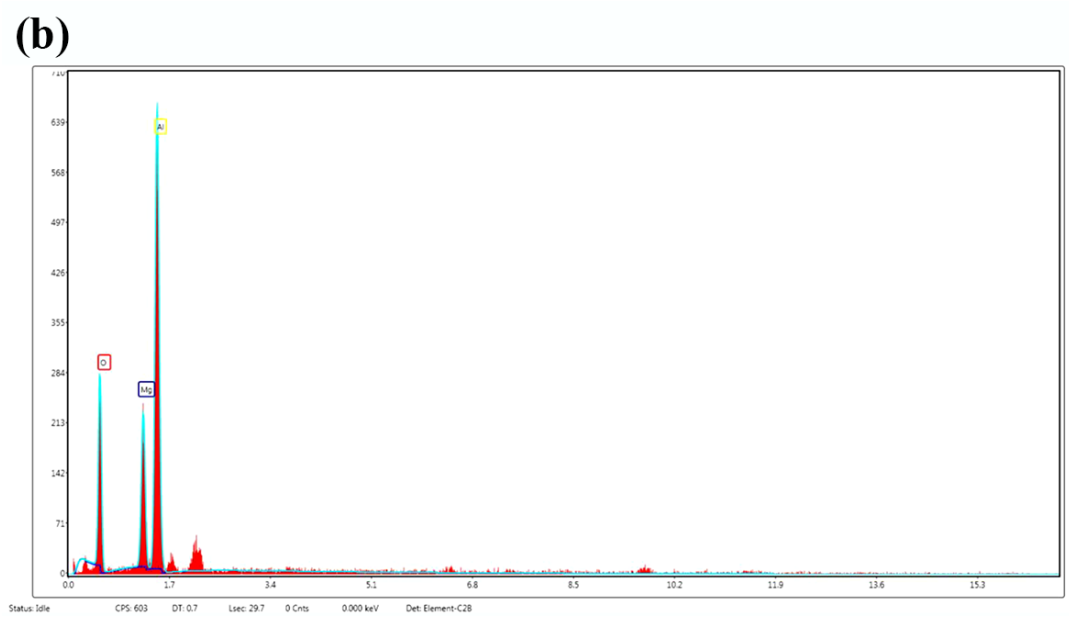
(b)
639
568
497
426
355
284
213
142
71
0
O
Mg
Al
0.0
1.7
3.4
5.1
6.8
8.5
10.2
11.9
13.6
15.3
Status: Idle
CPS: 603
DT: 0.7
Lsec: 29.7
0 Cnts
0.000 keV
Det: Element-C2B

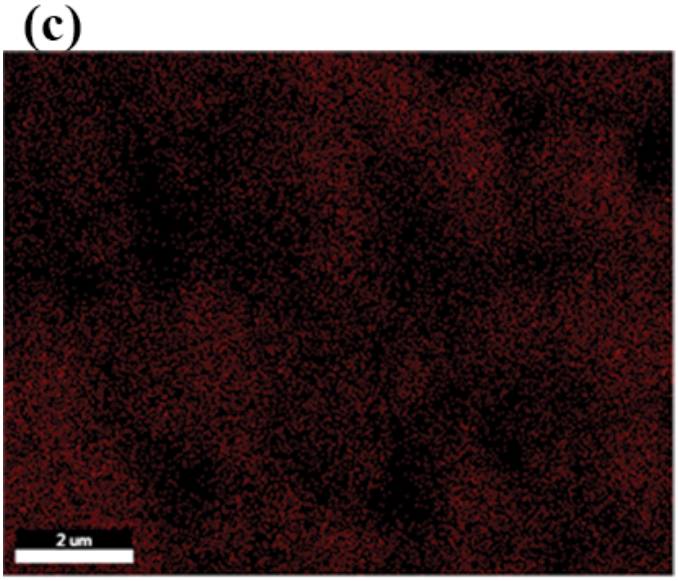
(c)
2 um

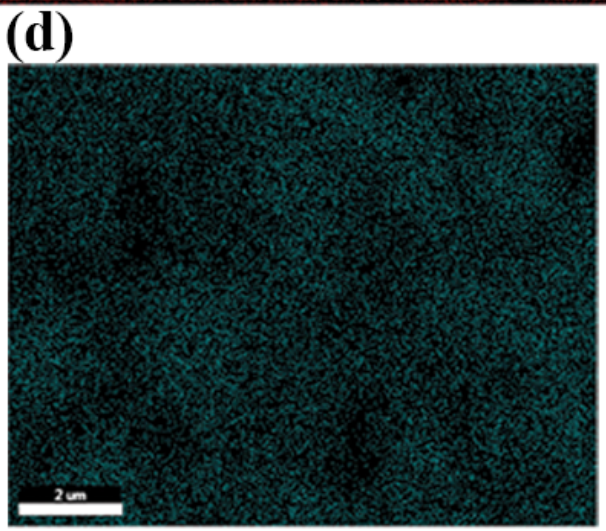
(d)
2 um

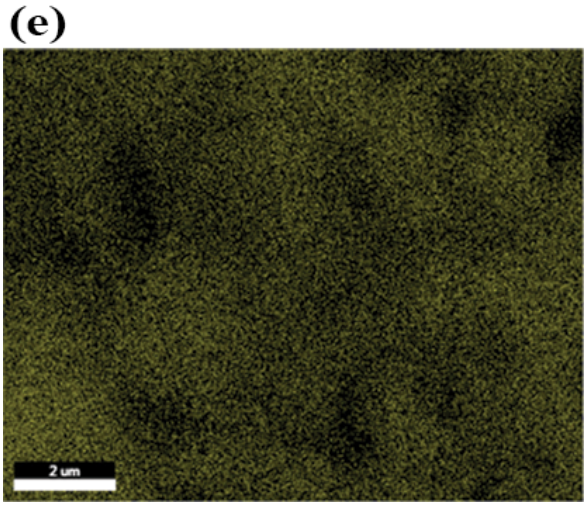

Fig. 11. (a) morphology of spinel $MgAl_2O_4$, (b) EDX analysis, (c), (d) and (e) X-ray map of spinel $MgAl_2O_4$

The SEM image of the mullite morphology is presented in Fig. 12(a). The image clearly shows the connection of cluster–like crystals composed of trapezoid particles. Fig. 12(b) and Table 2 confirm the results of EDX analysis for mullite. The result verifies that O, Si and Al, which are constituent elements related to the mullite, were synthesized using a combination of mechanical activation and three-step heat treatment techniques, and the non–availability of impurities in the synthesized mullite. Figs. 12(c-e) exhibits the results of the X-ray map of mullite. Fig. 12(c) shows the distribution of oxygen, demonstrating that the oxygen supplied from silica and alumina was put into the mullite structure. Fig. 12(d) illustrates the distribution of silicon and verifies a uniform distribution of Si^{4+}, resulting from the proper initial distribution of silica in mechanical activation. Similarly, Fig. 12(e) represents the distribution of Al and the existence of Al^{3+} which verifies the uniformity of the mullite structure.

Table 2. Results of EDX analysis of mullite

Element	Weight %	Atomic %	Net Int.
O K	43.37	56.64	267.68
Al K	40.34	31.24	788.46
Si K	16.29	12.12	195.27

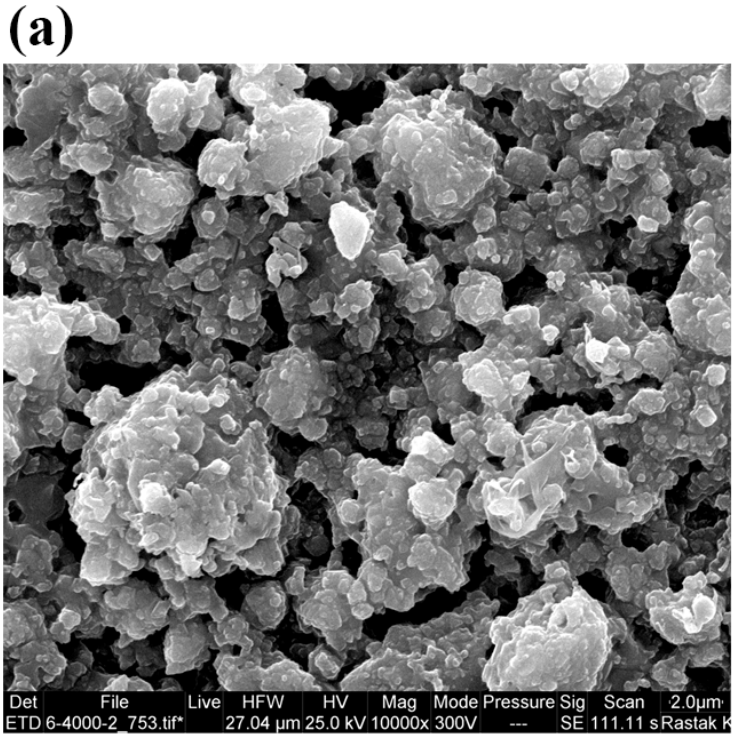

(b)

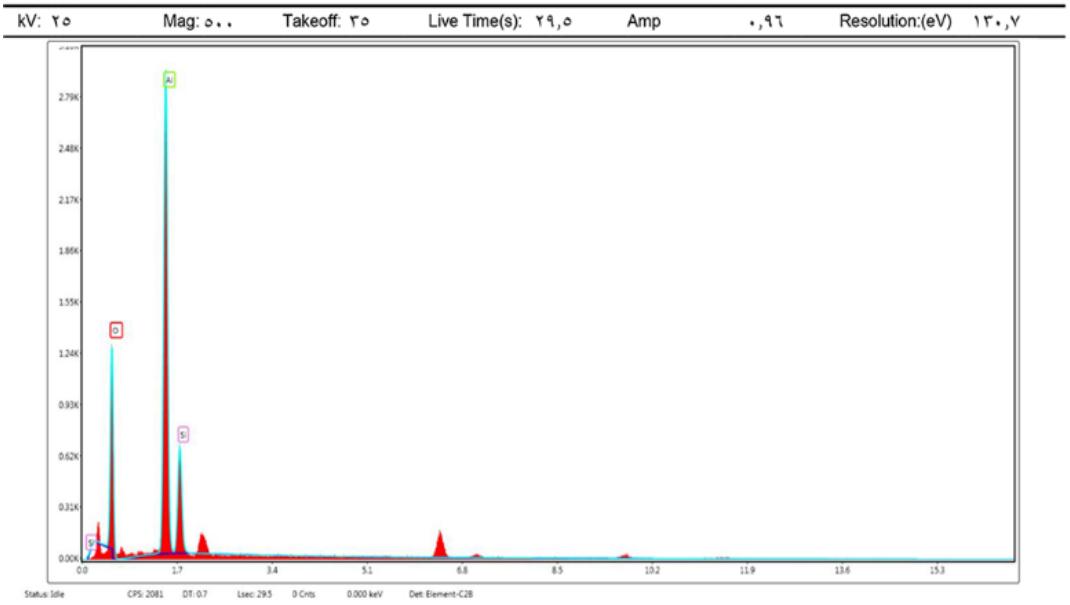
kV: ٢٥
Mag: ٥٠٠
Takeoff: ٣٥
Live Time(s): ٢٩,٥
Amp
٠,٩٦
Resolution:(eV) ١٣٠,٧
O
Si
0.0
1.7
3.4
5.1
6.8
8.5
10.2
11.9
13.6
15.3

(c)

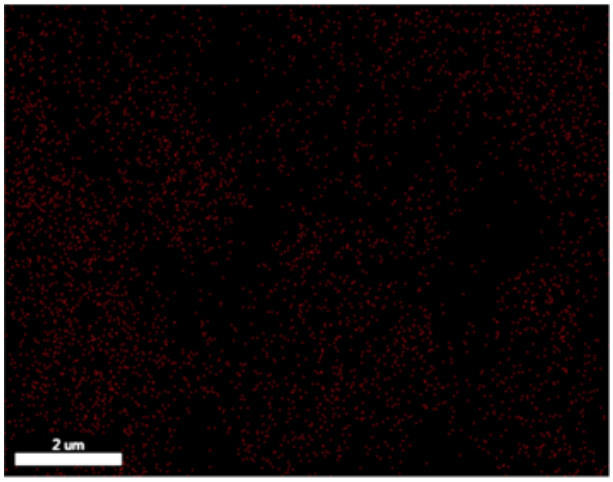
2 um

(d)

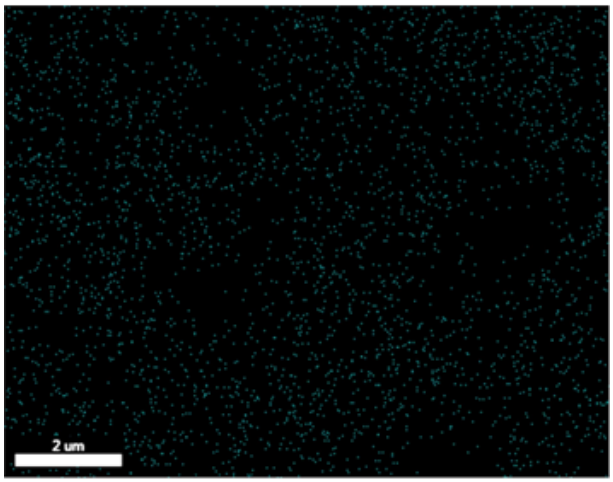
2 um

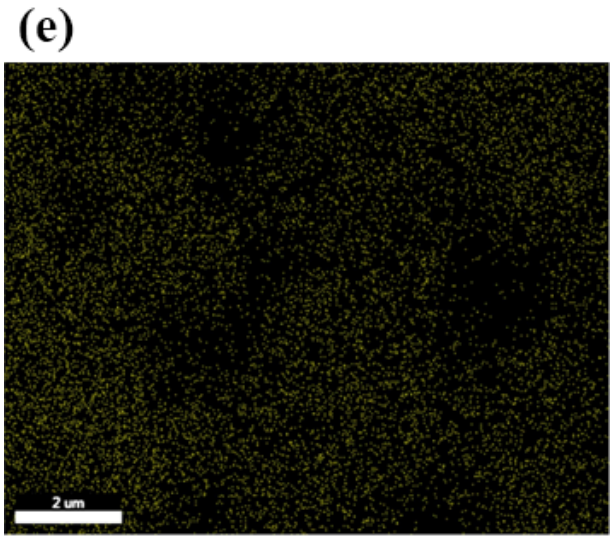

Fig. 12. (a) morphology of mullite, (b) EDX analysis, (c), (d) and (e) X-ray map of mullite

Fig. 13(a) depicts the morphology of the forsterite. The SEM image solidified the formation of white crystals in the glass matrix. The growth of the crystals was clearly observed in the glass matrix. Fig. 13(b) and Table 3 show the results of EDX analysis related to the synthesis of forsterite. The EDX analysis indicated O, Si and Mg, which verified the formation of the forsterite, the non–availability and using mechano-chemical and three-step heat treatment. Figs. 13(c-e) present the results related to the X-ray map of the forsterite. Fig. 13(c) illustrates the distribution of oxygen remaining from talc, magnesia, and silica that was put into the forsterite structure. Fig. 13(d) shows the distribution of magnesium (Mg^{2+}), implying the proper primary distribution of magnesia as a result of mechanical activation. Fig. 13(e) describes the distribution of silicon (Si^{4+}) resulting from mechanical activation and leading to the uniform forsterite structure.

Table 3. Results of EDX analysis of forsterite

Element	Weight%	Atomic%	Net Int.
O K	39.88	52.84	524.55
Mg K	15.23	13.28	554.68
Si K	44.89	33.88	1921.97

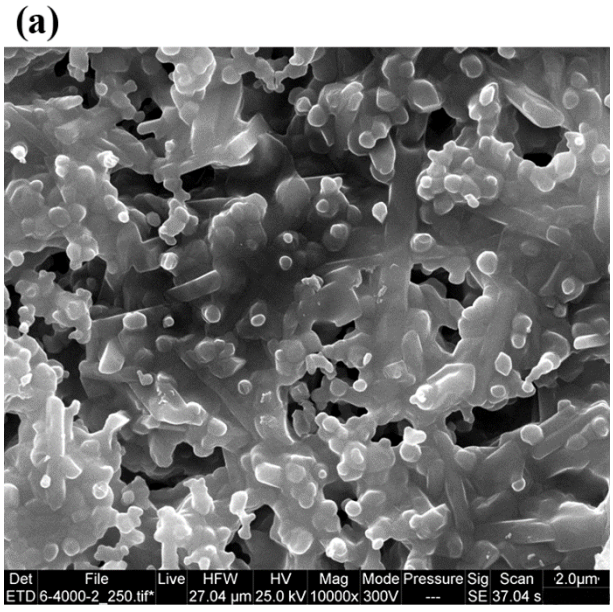

(b)

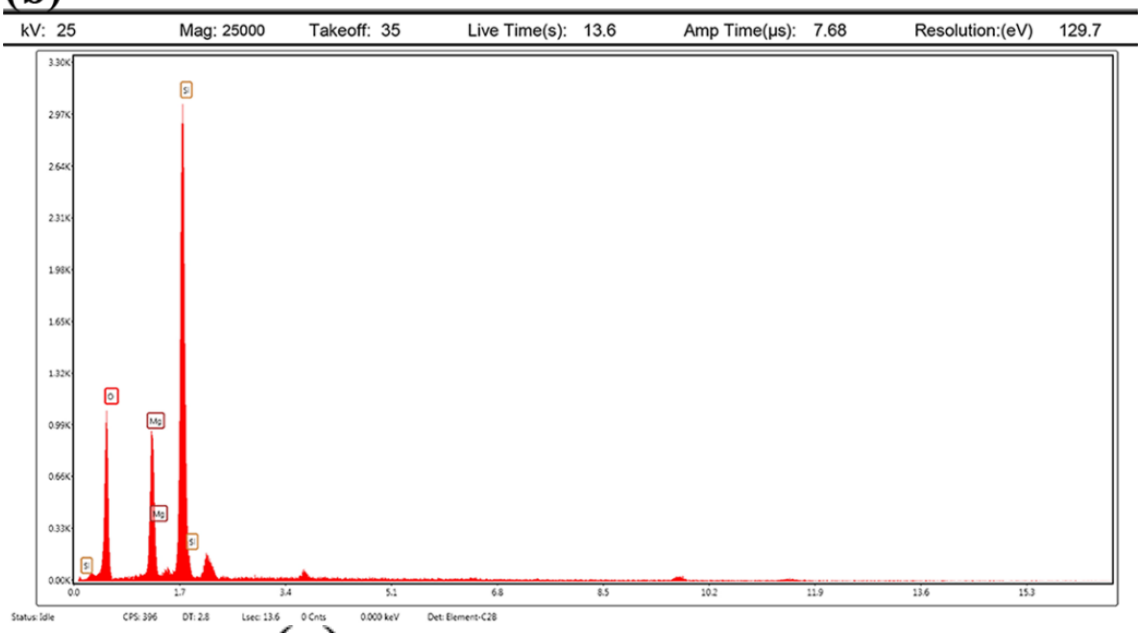
kV: 25
Mag: 25000
Takeoff: 35
Live Time(s): 13.6
Amp Time(µs): 7.68
Resolution:(eV) 129.7
O
Mg
Mg
Si
Si
Si
0.0
1.7
3.4
5.1
6.8
8.5
10.2
11.9
13.6
15.3

(c)

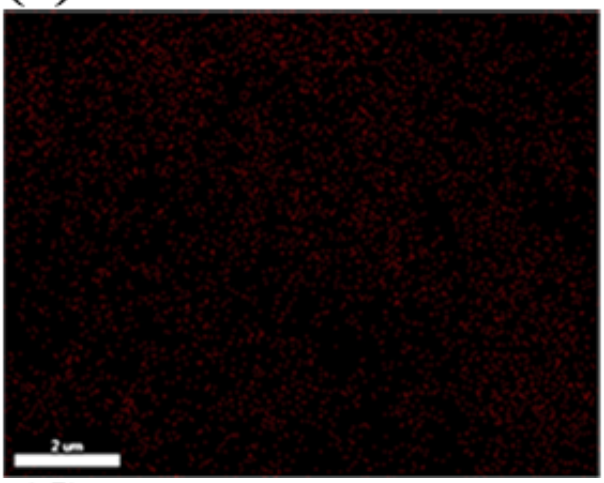
2 um

(d)

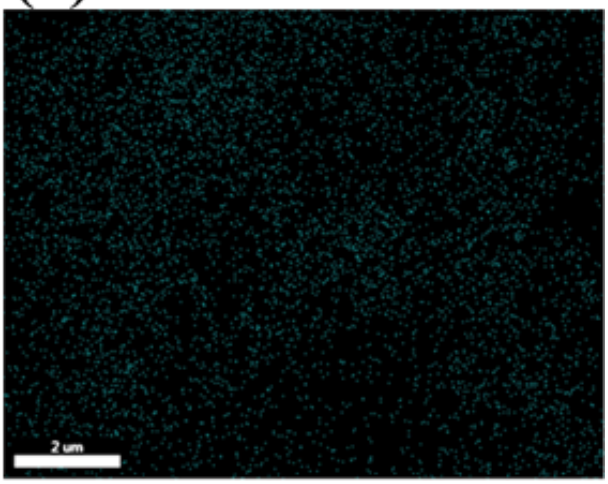
2 um

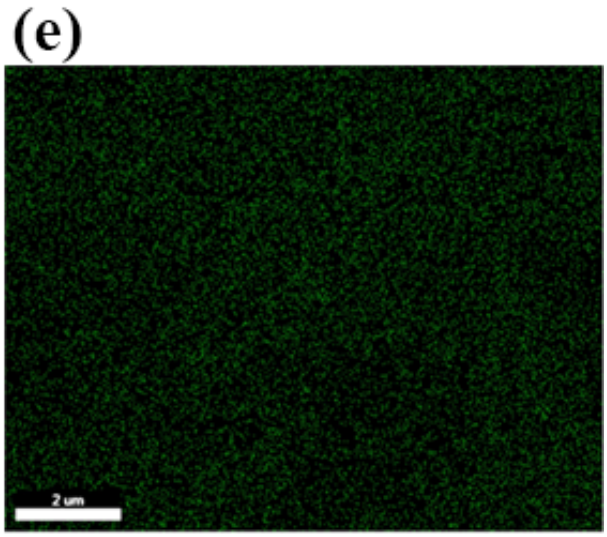

Fig. 13. (a) morphology of forsterite, (b) EDX analysis, (c), (d) and (e) X-ray map of forsterite

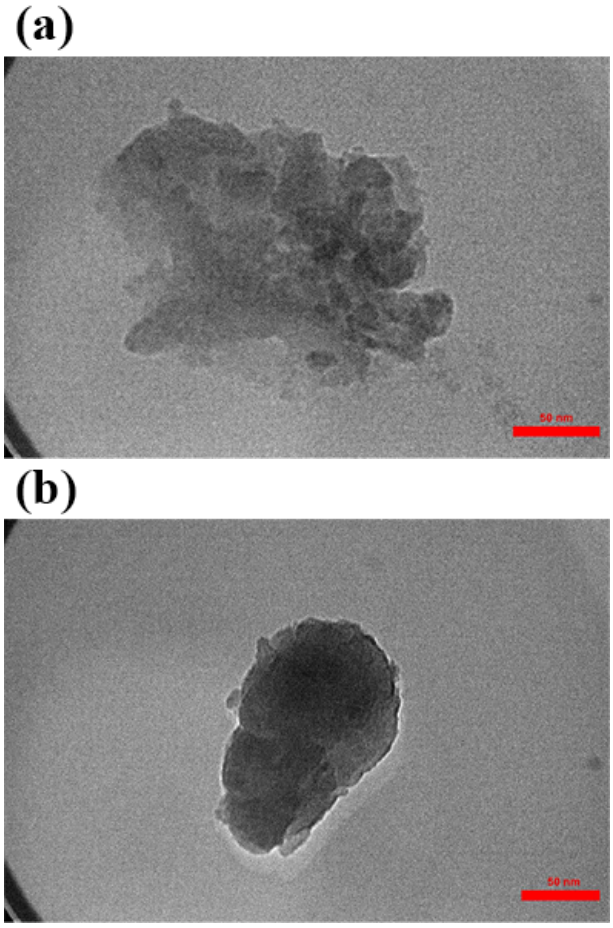

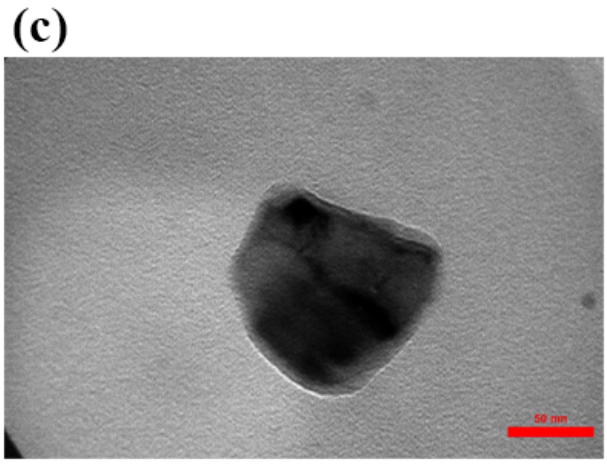

Fig. 14. TEM images: (a) spinel $MgAl_2O_4$, (b) mullite and (c) forsterite

Figs. 14(a-c) depict the TEM images of the synthesized spinel $MgAl_2O_4$, mullite, and forsterite. The TEM images confirm the particle size means being less than 100 nm for spinel $MgAl_2O_4$, mullite, and forsterite. The images also proved that the real sizes of the particles are less than 50 nm. Larger particles were developed because of nanoparticles agglomeration.

Table 4 reveals the results of the mean mechanical strength of the spinel $MgAl_2O_4$, mullite, and forsterite, which were obtained 378.33 ± 81.96, 216.33 ± 60.06, and 179.66 ± 85.49MPa, respectively. The results showed significant differences ($p<0.05$) and rendered high mechanical strength for the spinel $MgAl_2O_4$ in comparison to mechanical strength values for the mullite and forsterite. It can be claimed that strong ionic bonds exist between Mg–O and Al–O in the spinel structure. The ionic bonds enhance the mechanical strength related to the spinel. The data in Fig. 15 reveal that the combination of ionic bonds exists in the mullite structure through Al–O. The glass (SiO_2) exists in the mullite structure as the matrix. Therefore, Alumina (Al_2O_3) causes silicate networks to be broken which resulted in converting bridge oxygens to non–bridge oxygens (Fig. 15). The mechanism results in declining the mullite mechanical strength in comparison with the mechanical strength of the spinel to some extent. In addition, we know that only covalent bonds exist in the forsterite structure. Also, magnesium oxide could stimulate silicate networks and break them. This process causes the bridge oxygens to be converted to non-bridge oxygens (Fig. 16). The mechanism largely results in declining the mechanical strength related to forsterite. Although the spinel possessed a high mechanical strength in comparison with mullite and forsterite, the three nano–ceramics can be introduced as proper candidates for potential applications in porous materials, ceramics, and refractory industries.

Table 4. Results of mechanical strength of spinel $MgAl_2O_4$, mullite and forsterite

Specimen	Compressive Strength (MPa)
Spinel $MgAl_2O_4$	378 ± 81.96
Mullite	216.33 ± 60.06
Forsterite	179.66 ± 85.49

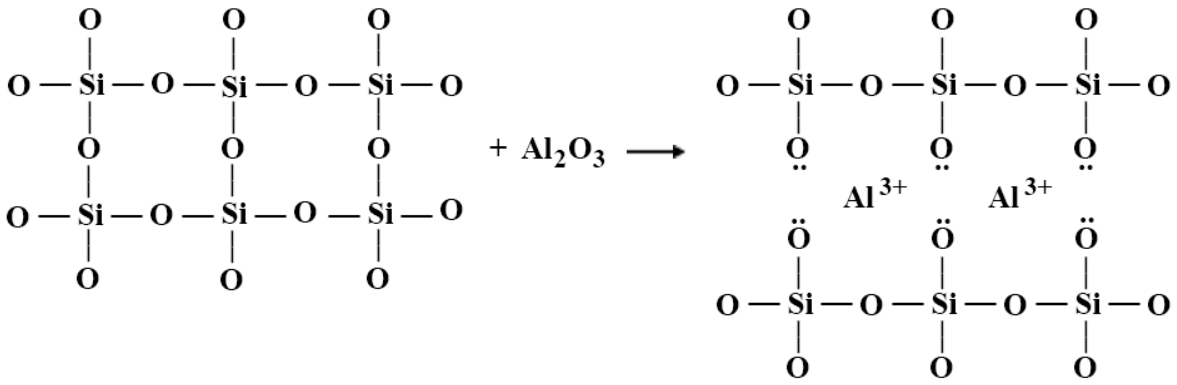

Fig. 15. Mechanism of bond-breaking of silicate networks by alumina

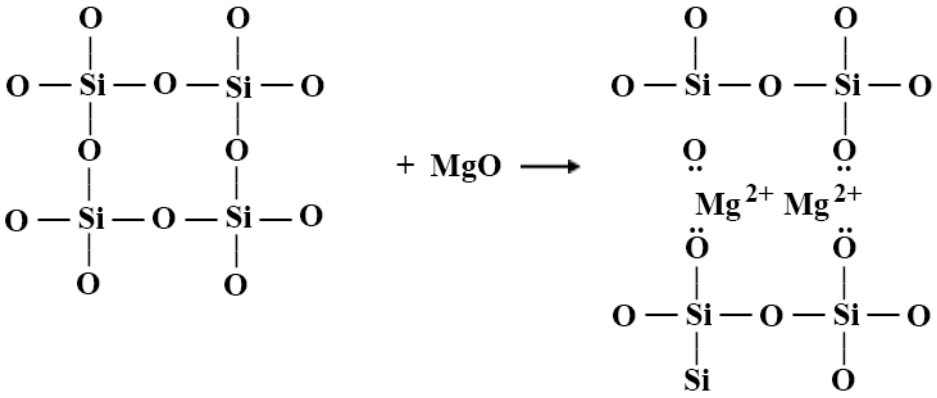

Fig. 16. Mechanism of bond-breaking of silicate networks by magnesia

4. Conclusion

The present research aimed at evaluating the formation reaction, substructure and mechanical behavior of spinel $MgAl_2O_4$, mullite and forsterite nanocrystallines via combining mechano-chemical and subsequent three-step heat treatment techniques. The results reveal that their formation can be carried out by low milling and declining annealing temperature. Phase transformation to form spinel $MgAl_2O_4$, mullite and forsterite was conducted at 1050 ^oC with respect to high activation energy and the strain energy saved in the particles by mechanical activation. The results rendered the crystallite sizes about 49.5, 70.71, and 47.8 nm and nanocrystallines formation with particles size of about 50 nm for spinel $MgAl_2O_4$, mullite, and forsterite. Mechanical strengths of nano-ceramics varied about 180-380 MPa, because of the existence of ionic and covalent bonds and the broken silicate networks in their structures. Taken together, with regard to the declining annealing temperature and enhancement of mechanical strength, nano-spinel $MgAl_2O_4$, nano-mullite, and nano-forsterite could be introduced as great candidates to be applied to porous materials, ceramics, and refractory industries.

References

[1] R. Lanos, I. Lazau, and P. Barvinschi, "Solution Combustion Synthesis of $MgAl_2O_4$ Using Fuel Mixtures", Mat. Res. Bull. J., Vol. 43, 2008, pp. 3408-3415.

[2] L. Duras, et. al., "$MgAl_2O_4$ Spinel Synthesis by Combustion and Detonation Reactions: a Thermochemical Evaluation", Euro. Ceram. Soc. J., Vol. 32, 2012 pp. 3161-3170.

[3] R. Salomao, M.O.C. Boas, and V.C. Pandolfelli, "Porous Alumina – Spinel Ceramics for High Temperature Applications", Ceram. Int. J., Vol. 37, 2011, pp. 1393-1399.

[4] A. Banerjee, et. al., "Structural Analysis on Spinel ($MgAl_2O_4$) for Application in Spinel – Bonded Castables", Ceram. Int. J., Vol. 35, 2009, pp. 381 – 390.

[5] Y.F. Liu, et. al., "Porous Mullite Ceramics from National Clay Produced by Gel-casting", Ceram. Int. J., Vol. 27, 2001, pp. 1-7.

[6] J. Bai, "Fabrication and Properties of Porous Mullite Ceramics from Calcined Carbonaceous Kaolin and Al_2O_3", Ceram. Int. J., Vol. 36, 2010, pp. 673-678.

[7] M.H. Talou. and M.A. Camerucci, "Processing of Porous Mullite Ceramics Using Novel Routes by Starch Cosolidation Casting", Euro. Ceram. Soc. J., Vol. 35, 2015, pp.1021-1030.

[8] O. Ebrahimpour, C. Dubois, and J. Chaouki, " Fabrication of Mullite-Bonded Porous SiC Ceramics via a Sol-gel Assisted In situ Reaction Bonding", Euro. Ceram. Soc. J., Vol. 34, 2014, pp. 237-247.

[9] T. Ebadzadeh, "Formation of Mullite from Precursor Powders: Sintering Microstructure and Mechanical Properties", Mat. Sci. Eng. J., Vol. A355, 2003, pp.56-61.

[10] H.J. Kleebe, et. al., "Conversion of Al_2O_3-SiO_2 Powder Mixtures to 3:2 Mullite Following the Stable or Metastable Phase Diagram", Euro. Ceram. Soc. J., Vol. 21, 2001, pp. 2521-2533.

[11] I.A. Aksay, D.M. Dabbs, and M. Sarikaya, "Mullite for Structural, Electronic and Optical Applications", Amer. Ceram. Soc. J., Vol. 74, 1991, pp. 2343-2358.

[12] C.Y. Chen, and W.H. Tuan, "The Processing Kaolin Powder Compact", Ceram. Int. J., Vol. 27, 2001, pp.795-800.

[13] Y.F. Chen, M.C. Wang, and M.H. Hon, "Transformation Kinetics for Mullite in Kaolin-Al_2O_3 ceramics", Mat. Res. J., Vol. 18, 2003, pp.1355-1362.

[14] Y.F. Liu, et. al., "Kinetics of the Reactive Sintering of Kaolinite-Aluminum Hydroxide Extrudate", Ceram. Int. J., Vol. 28, 2002, pp. 479-486.

[15] F. Sahnoune, et. al., "Algerian Kaolinite Used for Mullite Formation", Appl.Cla. Sci. J., Vol. 38, 2008, pp.304-310.

[16] T. Nezuka, et. al., "In situ Neutron Diffraction Investigation on the Phase Transformation Sequence of Kaolinite and Halloysite to Mullite", Phy. B J., Vol. 385-386, 2006, pp. 555-557.
[17] F. Tavangarian, R. Emadi, A. Shafiei, "Influence of Mechanical Activation and Thermal Treatment on Nanoparticle Forsterite Formation Mechanism", Pow. Tech. J., Vol. 198, 2010, pp. 412-416.
[18] F. Tavangarian, R. Emadi, "Synthesis of Nanocrystalline Forsterite Powder by Combined Mechanical Activation and Thermal Treatment", Mat. Res. Bull. J., Vol. 45, 2010, pp. 388-391.
[19] C.B. Abi, et. al., "Production of Forsterite from Serpentine-Effects of Magnesium Chloride Hexahydrate Addition", Adv. Pow. Tech. J., Vol. 26, 2015, pp. 947-953.
[20] F. Tavangarian, R. Emadi, "Effects of Mechanical and Chlorine Ion on Nanoparticle Forsterite Formation", Mat. Lett. J., Vol. 65, 2011, pp. 126-129.
[21] X. Zhang, and S. Li, "Mechanochemical Approach for Synthesis of Layered Double Hydroxides", Appl. Surf. Sci. J., Vol. 274, 2013, pp. 111- 123.
[22] M.F. Zawrah, H. Hamaad, S. Meky, "Synthesis and Characterization of Nano $MgAl_2O_4$ by the Co – Precipitated Method", Ceram. Int. J., Vol. 33, 2007, pp. 969 – 978.
[23] K.J.D. Mackenzie, et al., "Mechanochemical Synthesis and Sintering Behavior of Magnesium Aluminate Spinel", Mat. Sci. J., Vol. 35, 2000, pp. 5529 – 5535.
[24] L.B. Kong, J. Ma, and H. Huang, "$MgAl_2O_4$ Spinel phase Derived from Oxide Mixture Activated by a High – Energy Ball Milling Process", Mat. Lett. J., Vol. 56, 2002, pp. 238 – 243.
[25] T. Tsuzuki, and G. Paul, "Mechanochemical Synthesis of Nanoparticles", Mat. Sci. J., Vol. 39, 2004, pp. 5143 – 5146.
[26] A. Monshi, M. Foroughi, and M. Monshi, "Modified Scherrer Equation to Estimate More Accurately Nano-Crystallite Size Using XRD", Nan. Sci. and Eng. J., Vol. 2, 2012, pp. 154-160.